Neuromuscular Disorders 33 (2023) 951–963

Contents lists available at ScienceDirect

Neuromuscular Disorders

journal homepage: www.elsevier.com/locate/nmd

Functional characterization of *RYR1* variants identified in malignant hyperthermia susceptible individuals

Yuko Noda[a,b], Hirotsugu Miyoshi[b], Sofia Benucci[a], Asensio Gonzalez[c], Oliver Bandschapp[c], Thierry Girard[c], Susan Treves[a,d,*], Francesco Zorzato[a,d,*]

[a] Departments of Biomedicine and Neurology, Basel University Hospital, Hebelstrasse 20, Basel 4031, Switzerland
[b] Department of Anesthesiology, Hiroshima University Hospital, 1–2-3 Kasumi Minami-ku Hiroshima, 734-8551, Japan
[c] Anesthesiology, Spitalstrasse 21, Basel 4031, Switzerland
[d] Department of Life Science and Biotechnology, University of Ferrara, Via Borsari 46, Ferrara 44100, Italy

ARTICLE INFO

Article history:
Received 28 June 2023
Revised 25 October 2023
Accepted 30 October 2023

Keywords:
Ryanodine receptor
Malignant hyperthermia
Mutations
Calcium dysregulation
Diagnosis

ABSTRACT

Malignant hyperthermia is a pharmacogenetic disorder triggered by halogenated anesthetic agents in genetically predisposed individuals. Approximately 70 % of these individuals carry mutations in *RYR1*, the gene encoding the ryanodine receptor calcium channel of skeletal muscle. In this study, we performed functional analysis of 5 *RYR1* variants identified in members from 8 families who had been diagnosed by the IVCT. Of the 68 individuals enrolled in the study, 43 were diagnosed as MHS, 23 as MHN, and 2 individuals were not tested. Here we demonstrate that the 5 RyR1 variants cause hypersensitivity to RyR1 agonist-mediated calcium release. According to the EMHG scoring matrix these five genetic variants can be classified as follows: c.8638G>A (p.E2880K) and c.11314C>T (p.R3772W) likely pathogenic, c.11416G>A (p.G3806R), c.14627A>G (p.K4876R) and c.14813T>C (p.I4938T), pathogenic (RefSeq NM_000540.3). We propose that the newly functionally characterized *RYR1* variants, be included in the panel of variants to be used for the molecular diagnosis of MHS.

1. Introduction

Malignant hyperthermia (MH; OMIM# 145,600) is a life threatening pharmacogenetic disorder affecting skeletal muscle, triggered by volatile inhalation anesthetics and depolarizing muscle relaxants [1] The exposure of MH susceptible (MHS) individuals to trigger agents induces a severe dysregulation of skeletal muscle Ca^{2+} homeostasis resulting in the clinical features of an MH reaction, which include muscle rigidity, a rise in body temperature, metabolic acidosis and ultimately death [2,3]. Whilst some MHS individuals present mild muscle symptoms in their daily lives, or suffer from heat induced/exercise rhabdomyolysis [4,5], many others are asymptomatic and develop an MH reaction only after exposure to trigger agents under general anesthesia [1]. Thus, the diagnosis of MHS is important because it is cost effective and prevents the development of a life-threatening MH reaction. Indeed, MH reactions can be prevented in susceptible individuals by avoiding trigger agents and using non-volatile anesthetics during surgery. Although the introduction of dantrolene, an antagonist of skeletal muscle Ca^{2+} homeostasis dysregulation, has drastically reduced the mortality of MH, the death rate of MHS individuals exposed to MH trigger agents is still around 10 % [6–8].

To identify individuals prior to their exposure to trigger agents, family members of MHS individuals undergo the *in vitro* contracture test (IVCT) and/or molecular genetic testing. IVCT is the gold standard test to establish an individual's risk of MHS, but it is invasive since it requires an open muscle biopsy [9]. Based on the response of their muscles to *in vitro* stimulation with halothane and caffeine, individuals are classified as MHS (or MHShc) if their muscles respond abnormally to both halothane and caffeine, MHSh if their muscles respond abnormally to halothane, MHSc if their muscles respond abnormally to caffeine or MHN [10]. In addition to its invasiveness, muscle biopsies can be performed in adults under local regional anesthesia, which does not trigger MH, but not in children, as such diagnostic muscle biopsies are not usually performed under the age of ten years. For this reason, noninvasive molecular genetic testing tends to be preferred

* Corresponding authors at: Neuromuscular Research group, Department of Biomedicine, Lab 408 Hebelstrasse 20, 4031 Basel, Switzerland.
E-mail addresses: susan.treves@unibas.ch (S. Treves), fzorzato@usb.ch (F. Zorzato).

https://doi.org/10.1016/j.nmd.2023.10.019

[11], even though genetic heterogeneity and the relatively modest number of functionally characterized mutations with respect to the large number of potentially pathogenic variants reported to date, severely limit this genetic screening approach. Asides mutations in *RYR1*, the gene encoding the ryanodine receptor 1 (RyR1) Ca^{2+} channel of skeletal muscle sarcoplasmic reticulum, mutations in *CACNA1S,* the gene encoding voltage-dependent, L type, α 1S subunit and *STAC3,* the gene encoding Cysteine Rich Domain 3 protein are causally linked to the MHS phenotype [12,13]. Overall, variants in *RYR1, CACNA1S* and *STAC3* account for 50 to 80 % of all mutations identified in malignant hyperthermia susceptible individuals, with *RYR1* variants being the most common [14].

In recent years next-generation sequencing (NGS) has become faster, more accurate, and cost-effective, leading to its greater implementation, causing a paradigm shift in the diagnostic procedure of genetically heterogeneous disorders. The diagnosis of MHS is no exception, and genetic screening of MHS individuals and their family members has been facilitated. As a result, an increasing number of new genetic variants has been identified as possible causes of MHS. Dominant mutations in *RYR1* are responsible for approximately 75 % of all MHS cases and approximately 700 *RYR1* variants have been identified to date [15] but only 66 of these have been recognized as diagnostic by the European Malignant Hyperthermia Group (EMHG) (https://www.emhg.org/diagnostic-mutations). Such a big discrepancy is due to the fact that most genetic variants haven't been functionally evaluated. In order to be classified as pathogenetic, mutations need to meet specific criteria as defined by the EMHG (https://www.emhg.org/genetic-scoring-matrix), including scientific evidence of a direct causal relationship between the presence of the mutation and alteration of RyR1-mediated calcium release. Functional analysis for variants found in MHS patients has struggled to keep pace with the growing number of genetic variants discovered in the MHS population thanks to advancements in genetic analysis technology. The establishment of a functional defect of a RyR1 variant is a major bottleneck in its diagnostic inclusion, but is a basic condition required for a mutation to be included in the list of variants utilized for genetic diagnosis of MHS in patients and their family members. *In silico* prediction tools can be valuable in addressing this issue since they can provide structural insight and predictions based on data and algorithms. Several tools have emerged in the past few years and they are widely used to assess the potential pathogenicity of mutations identified through NGS. Each prediction tool possesses distinct characteristics and their accuracy improves when multiple tools are employed simultaneously. However, relying solely on predictive tools for mutation evaluation has limitations. Thus, experts recommend that the potential pathogenicity of a mutation should be made by considering a combination of factors, including mutation frequency, evolutionary conservation and functional analysis results [16].

Recently, the ClinGen Mutation Curation Expert Panel (VCEP) designated the American College of Medical Genetics and Genomics Society/Association of Molecular Pathologists (ACMG/AMP) criteria for the pathogenicity of *RYR1*-related MHS binomial disease entities [15]. Reports that classify *RYR1*-related MHS variants based on this criterion for their pathogenicity indicate that approximately 65 % of variants are still categorized as variant of uncertain significance (VUS), making the evaluation of MHS through genetic testing extremely challenging. Thus, continuous efforts should be directed towards augmenting the available data on *RYR1* variants through functional analysis and sharing of case materials. This would facilitate the reclassification of variants from VUS to either Likely Benign (LB)/Benign (B) or Likely Pathogenic (LP)/Pathogenic (P).

In order to fill the gap of unmet clinical needs in the identification of MHS individuals prior to their development of a life-threatening MH reaction, we have investigated the functional effect of five *RYR1* variants identified in patients and/or their family members, who had been diagnosed as MHS by the IVCT.

2. Materials and methods

2.1. Ethical considerations and patient selection

This study was approved by the Ethics committee of the Basel University Hospital (EKNZ 2014–065) and patients donated their muscle biopsy to the biobank of the Swiss Muscle Foundation (https://muskel-stiftung.ch/index.php/welcome/information-en) for the purpose of MH associated research. We investigated 68 individuals from 8 families with a positive history of MH without any reported clinical signs of neuromuscular diseases or exercise/heat intolerance. IVCT and DNA screening were performed on all individuals and their family members in order to identify causative *RYR1* variants on IVCT-positive individuals. Once a causative *RYR1* variant was identified in the family, other family members were tested for that variant only. If a *RYR1* variant not included as MH causative in the EMHG mutation panel (https://www.emhg.org/diagnostic-mutations) was found in an IVCT-positive individual, functional analysis was performed either on patient-derived myotube cultures when these were available or in HEK-293 heterologous cells transfected with a plasmid encoding the human RYR1 cDNA.

2.2. In silico *variant analysis*

Variant pathogenicity was evaluated with the web prediction tool REVEL (https://sites.google.com/site/revelgenomics/) included in the ACMG classification system [15]. Additionally, variants were analyzed with the following tools: SIFT (https://sift.bii.a-star.edu.sg/), PolyPhen-2 (http://genetics.bwh.harvard.edu/pph2/), Mutation Taster (https://www.mutationtaster.org/), and CADD (https://cadd.gs.washington.edu/info) to predict their pathogenicity.

2.3. Variant classification

Pathogenicity of variants included in this study was classified based on the ECMG (https://www.emhg.org/genetic-scoring-matrix) and the ACMG criteria as described in VCEP [15]. According to the EMHG guidelines, there are three categories of pathogenetic variant classification: strong (PSa, PSb), moderate (PMa, PMb) and supporting (PSa, PSb, PSc) and three categories of benign variant classification: stand- alone (BAa, BAb, BAc), strong (BSa, BSb) and supporting (BPa). A pathogenic variant is defined by at least 1 PS criterion and 2 PP criteria and a likely pathogenic variant is defined as at least 1 PM criterion and 2 PP criteria. A benign variant is defined by at least one BA criterion or 2 x BS criteria and a likely Benign variant is defined by one BS criterion and one BP criterion. A variant that does not meet any of the above criteria is defined as VUS (https://www.emhg.org/genetic-scoring-matrix).

According to VECP guidelines, each pathogenic criterion is weighted as very strong (PS2/PM6_Very Strong), strong (PS1, PS2/PM6_Str, PS3, PS4, PP1_Str), moderate (PM1, PM5, PS2/PM6_Mod, PS3_Mod, PS4_Mod, PP1_Mod, PP3_Mod), or supporting (PP1, PS2/PM6_Sup, PS3_Sup, PS4_Sup, PM_1Sup) and each benign criterion is weighted as stand-alone (BA1), strong (BS1, BS2), moderate (BS2_Mod, BS3_Mod) or supporting (BP2, BP4, BP7, BS3_Sup). To determine pathogenicity, all criteria that are applicable to the variant are summed and the Odds of Pathogenicity is calculated using a formula developed by Tavtigian et al. [17] as a Bayesian Classification Framework. In the present

report, the posterior probability was calculated using the formula of the ACMG guidelines and pathogenicity was determined accordingly [15].

2.4. Preparation of patient myotubes and intracellular Ca^{2+} measurements

Primary muscle cultures were established as previously described from pieces of muscle biopsies leftover from the IVCT [18–20]. When a sufficient number of myoblasts had grown and the cultures were approximately 80 % confluent, cells were trypsinized and transferred onto 10 mm diameter, 0.17 mm thick laminin-treated glass coverslip. Once the myoblasts reached 90 % confluency, the medium was changed to differentiation medium [20] and 7–10 days later, once multinucleated myotubes were visible, cells were loaded with the fluorescent Ca^{2+} indicator fura-2 (final concentration 5 μM) for 30 min at 37 °C. The coverslips were mounted onto a thermostatically controlled (37 °C) perfusion chamber which was continuously perfused with Krebs Ringer solution (140 mM NaCl, 5 mM KCl, 1 mM $MgSO_4$, 10 mM HEPES, 1 mM Na_2HPO_4, 5.5 mM D-(+)-Glucose (pH 7.4) containing 2 mM $CaCl_2$. Myotubes were individually stimulated by means of a 12- or 8-way 100-mm diameter quartz micromanifold computer controlled microperfuser (ALA Scientific instruments, Westbury, NY), by the addition of different concentrations of KCl (0, 7.5, 10, 20, 40, 60, and 100 mM) or 4-chloro-*m*-cresol (0, 75, 150, 300, 450, 600, 750, and 900 μM) in Krebs Ringer solution. Fluorescence measurements were acquired using an inverted Zeiss Axiovert S100 TV fluorescent microscope equipped with a 20x water-immersion FLUAR objective (0.17 NA), filters (BP 340/380, FT 425, BP 500/530) and attached to a Cascade 125 + CCD camera. Changes in fluorescence were analysed using Metamorph imaging system and the average pixel value for each cell was measured [19,20]. The average change in fluorescence elicited by the agonist (either KCl or 4-chloro-m-cresol) was calculated and used to construct dose response curves using Origin (Microcal Software, Inc Northampton, MA, USA).

2.5. RYR1 *cDNA constructs*

The human *RYR1* cDNA was subcloned in the bi-cistronic pIRES2-DsRed2 vector (Clontech Laboratories), which allows the expression of the cytoplasmic DsRed2 protein, along with the RyR1 protein. The emission and excitation spectra of DsRed are 558 and 583 nm, respectively and thus there is no interference with fura-2-based calcium measurements (excitation 340 and 380 nm, emission 510 nm). The cloning of the full-length rabbit skeletal muscle *RYR1* cDNA-pBluscript SK(-) has been previously described [21]. Human *RYR1* cDNA was synthesized using mRNA isolated from human skeletal muscle as a template (transcript variant 2, NCBI Reference Sequence: NM_001042723.1). The full length RYR1 cDNA was assembled through a series of subcloning steps in which fragments of different sizes (from 600bp-2629 bp) were inserted individually into the bacterial plasmid pBSK(-), this was followed by ligation and joining one insert at a time in order to obtain the full length construct. The different fragments were sequenced in order to confirm the *RYR1* cDNA primary sequence.

2.6. Expression of RyR1 in HEK-293 cells and immunoblotting

HEK-293 cells were plated in 100 mm tissue culture plates (Beckton Dickinson number) and grown at 37 °C and 5 % CO_2 in MEM and Earl's medium containing 10 % fetal bovine serum, GlutaMAX™ (ThermoFisher Scientific, Waltham, MA), and Penicillin-Streptomycin (ThermoFisher Scientific, Waltham, MA) until 70–80 % confluent. Cells were transfected with wild-type or mutant human *RYR1* cDNAs (p.G3806R, p.K4876R, and p.I4938T) using the ESCORT™ IV Transfection Reagent (Sigma-Aldrich, Germany) according to the manufacturer's recommendations. Three days after transfection, cells were harvested and microsomal proteins were prepared as described [22]. The protein concentration in the microsomes was determined using the Bio Rad protein assay dye reagent concentrate (BioRad Cat N°5,000,006). Western blots were performed as previously described [23]. Membranes were probed with rabbit monoclonal anti-RyR1 antibodies (1:1000 in TBST) (D4E1, #8153, Cell Signaling Technology, Danvers, MA, USA) followed by incubation with horseradish peroxidase-conjugated protein G (1:200,000 in TBST) (ThermoFisher Scientific, Waltham, MA) and the immunopositive bands were visualized using the enhanced chemiluminescence reagent WesternBright ECL- HRP Substrate (Witec AG, Sursee, Switzerland).

2.7. Intracellular calcium $[Ca^{2+}]_i$ measurements of transfected HEK-293 cells

For intracellular Ca^{2+} measurements, HEK-293 cells were cultured on 10 mm glass coverslips and transfected with the wild-type *RYR1* cDNA or the *RYR1* cDNA variants (c.11416G>A p.G3806R, c.14627A>G p.K4876R, and c.14813T>C p.I4938T subcloned in the bi-cistronic pIRES2-DsRed2 vector using Escort V liposomes (5 μg cDNA/coverslip). Seventy two h post transfection intracellular Ca^{2+} measurements were performed in cells loaded (40 min at 37 °C) with the ratiometric fluorescence calcium indicator fura-2/AM (Invitrogen). The coverslips were transferred to the perfusion chamber as outlined above for myotubes and perfused with Krebs Ringer Solution containing 2 mM Ca^{2+}. To identify transfected cells which are positive for the cytosolic DsRed fluorescent protein, cells were excited at 540 nm and fluorescence emission visualized at 575–640 nm. Using the same field, the dichroic filter was switched to BP 340/380, FT 425, BP 500/530 and the cells were analyzed for changes in $[Ca^{2+}]$ by monitoring fura-2 fluorescence in response to the application of 600 μM 4-chloro-m-cresol. Since only those cells that were positive for DsRed were considered successfully transfected, only red fluorescent cells were used for $[Ca^{2+}]_i$ measurements. Changes in $[Ca^{2+}]_i$ elicited by different concentrations of 4-chloro-m-chresol were performed as described above for myotubes.

2.8. Structural analysis of the position of the mutations inside the RyR1 sequence

Analysis and graphical representation of the RyR1 variants was performed with the use of Pymol software (The PyMOL Molecular Graphics System, Version 2.5.2, Schrödinger, LLC) or Chimera software (UCSF Chimera, production Version 1.16) [24] Highest probability rotamers were chosen among the Dunbrack 2010 backbone-dependent rotamer library [25] and subsequently clashes/H bonds were investigated. For the present investigation, cryo-EM resolved protein structures with the following PDB ID were used: 5T15 (resolution of 3.6 Å) and 5TAL (resolution of 4.6 Å) [26,27].

2.9. Data analysis and statistical analysis

For human myotubes, dose response curves were generated as previously described [20]. Data were normalized for the highest mean ΔF values obtained at a given concentration of KCl or 4-cmc, which was considered 100%. Experiments were performed on myotubes from 3 MHS patients carrying either the p.E2880K, the p.R3772W or the p.I4938T *RYR1* mutations and from 2 control

individuals (MHN) from family 1 and family 8. Myotubes from other mutation bearing family members or from non-mutation bearing individuals were not available. Cells were tested on 3 different days and the mean ΔF was averaged and used to plot sigmoidal dose response curves and to calculate the half-maximal effective concentration (EC_{50}), using Origin 6.0 (Microcal Software Inc., Northapmton, MA, USA). To construct 4-chloro-*m*-cresol (4-cmc) dose-response curves for the calcium response of HEK-293 cells, data were normalized to the highest mean ΔF values obtained at a given concentration of 4-cmc, which was considered 100 %. Statistical significance between EC_{50} values of each variant-transfected cells and that of human WT-*RYR1* cDNA transfected cells were compared using one-way analysis of variance (ANOVA). A P value < 0.05 was considered to be statistically significant. For comparisons of resting [Ca^{2+}], analysis was performed with PRISM 8.0 software (GraphPad Software, San Diego, CA) and mean values were compared using Dunnet's multiple comparison test a P value < 0.05 was considered statistically significant.

3. Results

3.1. DNA screening and genotype-phenotype correlation of the individuals carrying each variant

Five *RYR1* variants, namely c.8638G>A (p.E2880K), c.11314C>T (p.R3772W), c.11416G>A (p.G3806R), c.14627A>G (p.K4876R) and c.14813T>C (p.I4938T) were found in 8 MHS families. Of these, four including p.R3772W, p.G3806R, p.K4876R and p.I4938T, were previously reported as possible MHS candidate mutations and/or as likely pathogenic [28–30], but were never functionally tested. Fig. 1 (panels A to D) and Table 1 show the family trees and individuals in whom each variant was found, the number of families carrying the genetic variants, the results of genetic testing and of the IVCT for individuals with each variant. As shown, a total of 68 individuals from 8 families included in this study were genetically tested and/or tested by the IVCT as indicated in Table 1. The 8 families were unrelated, ensuring their independence in the context of the functional investigations. Altogether, there were nine patients with a wild type (WT) *RYR1* genotype who had positive IVCT results (8 MHSh and 1 MHShc) while two patients one harboring the c.8638G>A (p.Q2880K) variant and the other the c.14813T>C (p.I4938T) variant, were categorized as MHN as per negative IVCT results.

In detail, the p.E2880K mutation was found at the heterozygous state in 14/21 family members from 4 unrelated families; of the mutation carriers, 9 were classified as MHShc, 3 MHSh and 1 MHN with the IVCT while 1 could not be classified due to lack of IVCT testing (Fig. 1E). There were a total of 3/21 discordant cases: 2 patients were genotype (-) but IVCT (+) and 1 patient was genotype (+) but IVCT (-). The p.R3772W mutation was only identified in 1 MHS individual (Family 5, Fig. 1E). The p. G3806R was found at the heterozygous state in 14/32 family members from 1 family; of the mutation carriers, 9 were classified as MHShc and 5 as MHSh by the IVCT (Fig. 1E). One patient did not undergo genetic testing. There were 5/31 genotype (-) IVCT (+) discordant cases. The p.K4876R mutation was found at the heterozygous state in 3/3 family members from 1 family; of the mutation carriers 2 were classified as MHShc and 1 as MHSh by the IVCT (Fig. 1E). There was no discordance, supporting the pathogenicity (PP1_Sup) of this variant. The p.I4938T mutation was found at the heterozygous state in 5/11 family members from 1 family; of the mutation carriers 2 were classified as MHShc and 2 as MHSh and 1 as MHN by the IVCT (Fig. 1E). There were 3/11 discordant cases: genotype (-) IVCT (+) in 2 patients and genotype (+) IVCT (-) in 1 patient.

Table 1
MH status, family number, *RYR1* mutation and RyR1 substitution in individuals enrolled in the present investigation.

N°	Family N°	Indications for gene testing	Nucleotide change	Amino acid change	Genetic Result	IVCT result
1	1	MH family	c.8638G>A	p.Q2880K	wild-type	MHSh
2	1	MH family	c.8638G>A	p.Q2880K	wild-type	MHN
3	1	MH family	c.8638G>A	p.Q2880K	wild-type	MHN
4	1	MH family	c.8638G>A	p.Q2880K	heterozygous	MHSh
5	1	MH family	c.8638G>A	p.Q2880K	heterozygous	MHShc
6	1	MH family	c.8638G>A	p.Q2880K	wild-type	MHSh
7	1	MH-event	c.8638G>A	p.Q2880K	heterozygous	MHShc
8	1	MH family	c.8638G>A	p.Q2880K	heterozygous	MHShc
9	1	MH family	c.8638G>A	p.Q2880K	wild-type	MHN
10	2	MH family	c.8638G>A	p.Q2880K	heterozygous	MHShc
11	2	MH family	c.8638G>A	p.Q2880K	heterozygous	MHShc
12	2	MH family	c.8638G>A	p.Q2880K	wild-type	MHN
13	2	MH family	c.8638G>A	p.Q2880K	heterozygous	MHShc
14	3	MH-event	c.8638G>A	p.Q2880K	heterozygous	MHShc
15	3	MH family	c.8638G>A	p.Q2880K	heterozygous	MHN
16	3	MH family	c.8638G>A	p.Q2880K	heterozygous	MHShc
17	3	MH family	c.8638G>A	p.Q2880K	heterozygous	MHShc
18	3	MH family	c.8638G>A	p.Q2880K	heterozygous	MHSh
19	3	MH family	c.8638G>A	p.Q2880K	heterozygous	MHSh
20	3	MH family	c.8638G>A	p.Q2880K	wild-type	MHN
21	4	MH-event	c.8638G>A	p.Q2880K	heterozygous	n.d.
22	5	MH-event	c.11314C>T	p.R3772W	heterozygous	MHShc
23	6	MH family	c.11416G>A	p.G3806R	heterozygous	MHSh
24	6	MH family	c.11416G>A	p.G3806R	wild-type	MHN
25	6	MH family	c.11416G>A	p.G3806R	heterozygous	MHSh
26	6	MH family	c.11416G>A	p.G3806R	wild-type	MHN
27	6	MH family	c.11416G>A	p.G3806R	heterozygous	MHShc
28	6	MH family	c.11416G>A	p.G3806R	wild-type	MHN
29	6	MH family	c.11416G>A	p.G3806R	heterozygous	MHShc
30	6	MH family	c.11416G>A	p.G3806R	wild-type	MHSh
31	6	MH family	c.11416G>A	p.G3806R	heterozygous	MHShc
32	6	MH family	c.11416G>A	p.G3806R	heterozygous	MHShc
33	6	MH family	c.11416G>A	p.G3806R	wild-type	MHN
34	6	MH family	c.11416G>A	p.G3806R	wild-type	MHSh
35	6	MH family	c.11416G>A	p.G3806R	wild-type	MHN
36	6	MH family	c.11416G>A	p.G3806R	heterozygous	MHShc
37	6	MH family	c.11416G>A	p.G3806R	wild-type	MHN
38	6	MH family	c.11416G>A	p.G3806R	wild-type	MHN
39	6	MH family	c.11416G>A	p.G3806R	heterozygous	MHSh
40	6	MH family	c.11416G>A	p.G3806R	heterozygous	MHSh
41	6	MH family	c.11416G>A	p.G3806R	wild-type	MHN
42	6	MH family	c.11416G>A	p.G3806R	wild-type	MHSh
43	6	MH family	c.11416G>A	p.G3806R	heterozygous	MHSh
44	6	MH family	c.11416G>A	p.G3806R	wild-type	MHN
45	6	MH family	c.11416G>A	p.G3806R	wild-type	MHN
46	6	MH family	c.11416G>A	p.G3806R	wild-type	MHN
47	6	MH family	c.11416G>A	p.G3806R	wild-type	MHSh
48	6	MH family	c.11416G>A	p.G3806R	wild-type	MHSh
49	6	MH family	c.11416G>A	p.G3806R	heterozygous	MHShc
50	6	MH family	c.11416G>A	p.G3806R	wild-type	x
51	6	MH family	c.11416G>A	p.G3806R	heterozygous	MHShc
52	6	MH family	c.11416G>A	p.G3806R	heterozygous	MHShc
53	6	MH family	c.11416G>A	p.G3806R	wild-type	MHN
54	6	MH family	c.11416G>A	p.G3806R	heterozygous	MHShc
55	7	MH family	c.14627A>G	p.K4876R	heterozygous	MHSh
56	7	MH family	c.14627A>G	p.K4876R	heterozygous	MHShc
57	7	MH-event	c.14627A>G	p.K4876R	heterozygous	MHShc
58	8	MH family	c.14813T>C	p.I4938T	wild-type	MHN
59	8	MH family	c.14813T>C	p.I4938T	heterozygous	MHSh
60	8	MH family	c.14813T>C	p.I4938T	wild-type	MHSh
61	8	MH family	c.14813T>C	p.I4938T	wild-type	MHN
62	8	MH family	c.14813T>C	p.I4938T	wild-type	MHN
63	8	MH family	c.14813T>C	p.I4938T	heterozygous	MHN
64	8	MH family	c.14813T>C	p.I4938T	wild-type	MHN
65	8	MH family	c.14813T>C	p.I4938T	heterozygous	MHSh
66	8	MH family	c.14813T>C	p.I4938T	heterozygous	MHShc
67	8	MH family	c.14813T>C	p.I4938T	heterozygous	MHShc
68	8	MH family	c.14813T>C	p.I4938T	wild-type	MHShc

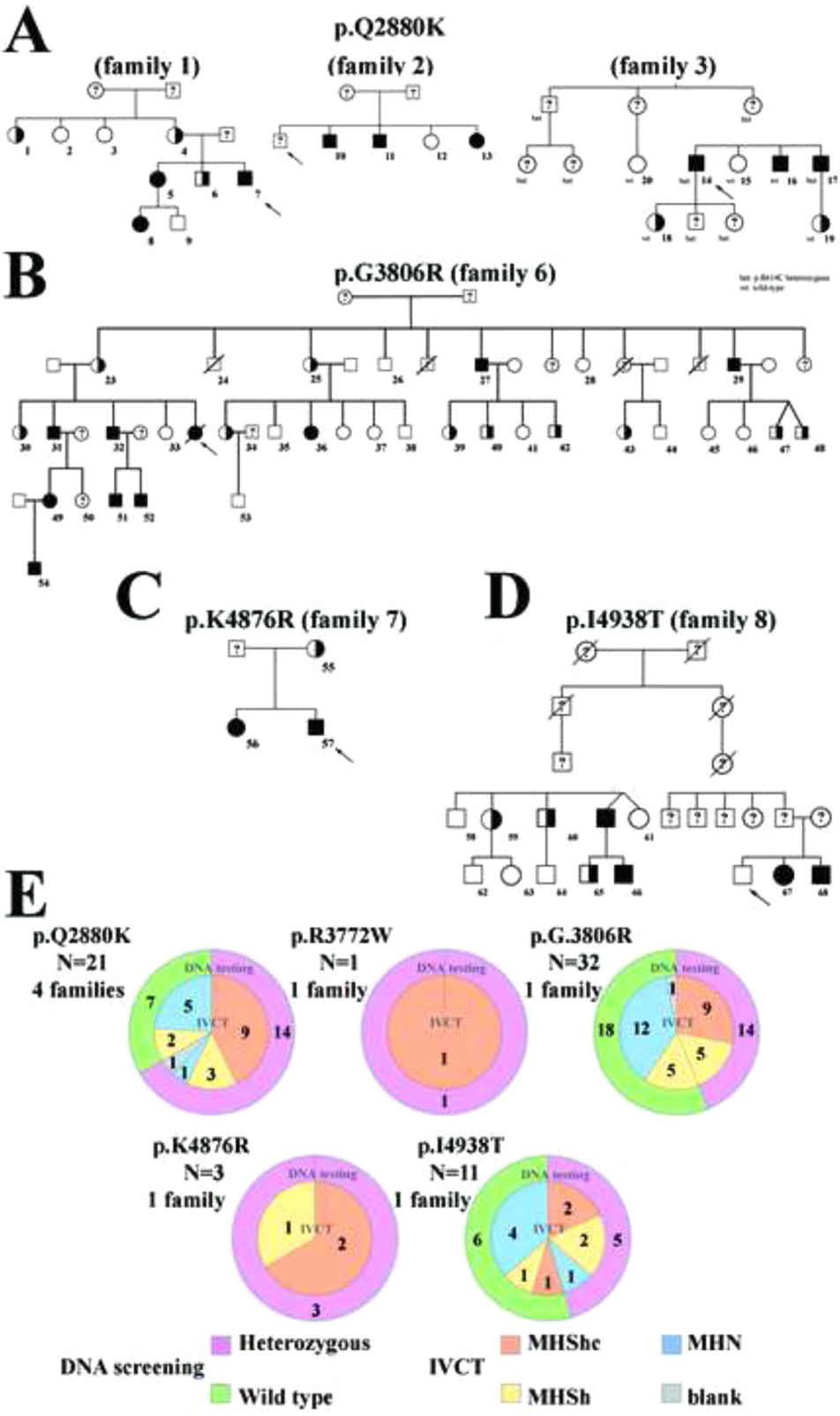

Fig. 1. Family trees and genotype-phenotype correlations of the individuals enrolled in this study. A. to D. Family trees of families 1,2,3,6,7 and 8 in whom the *RYR1* gene variants were found in this study. Arrow: MH-onset individual. Full black symbols: MHShc male/female. Half black symbols: MHSh male/female. Empty symbols: MHN male/female (negative IVCT). The presence of a "?" within the symbol denominates unknown IVCT status. **E**. Results of genetic testing and IVCT for individuals with each variant are shown in the double-pie charts for each gene variant. The outer circles show the results of the genetic testing (green WT, lilac heterozygous mutation carriers), and the inner circles show the results of the IVCT. The numbers within the circles indicate number of individuals tested. It is noteworthy that for 3 individuals there is a discrepancy between the IVCT result and genotype (1 heterozygous + negative IVCT in p.E2880K, 1 heterozygous + negative IVCT in p.I4938T, and 1 wild-type + MHS IVCT in p.I4938T).

Table 2
EC_{50} values for KCl and 4-cmc calcium release in myotubes carrying the WT RyR1 and the p.E2880K, p.R3772W and p.I4938T RyR1 variants.

	KCl EC_{50} (mM)	4-cmc EC_{50} (µM)
Control 01	18.5 ± 2.2	358.0 ± 46.5
Control 02	22.5 ± 12.2	310.0 ± 40.3
p.E2880K	14.5 ± 5.1**	292.9 ± 45.0**
p.R3772W	15.7 ± 0.6**	249.6 ± 47.8**
p.I4938T	18.1 ± 2.4	400.3 ± 52.6**

The EC_{50} value to KCl and 4-cmc of myotubes carrying the p.E2880K and p.R3772W variants are significantly reduced as compared to control myotubes from control (MHN) individuals
** $P < 0.01$,

Table 3
EC_{50} values for 4-cmc calcium release in HEK-293 expressing WT RyR1 and HEK-293 cells transfected with the p.G3806R, p.K4876R and p.I4938T RyR1 variants.

	EC_{50} (µM)	P value
WT	242.1 ± 12.3	< 0.0001****
p.G3806R	204.3 ± 14.1	< 0.0001****
p.K4876R	208.9 ± 12.3	< 0.0001****
p.I4938T	191.1 ± 30.1	< 0.0001****

The EC_{50} value of HEK-293 cells transfected with the p.G3806R, p.K4876R and p.I4938T RYR1 variants are significantly reduced as compared with that of WT. Statistically significant difference from WT are denoted by
**** ($P < 0.0001$).

3.2. In silico *genetic analysis of identified variants*

The 4 variants (p.E2880K, p.G3806R, p.K4876R and p.I4938T) had a REVEL score > 0.85, supporting their pathogenicity (PPb/PP3_Mod) [31]. Results of pathogenicity estimation by *in silico* prediction tools other than REVEL are shown in Supplementary Table 1.

3.3. *Functional properties of myotubes from individuals carrying p.E2880K, p.R3772W and p.I4938T RyR1 variants*

Muscle biopsies from patients carrying the 3 *RYR1* variants and from 2 wild type controls were used to generate primary muscle cell cultures. Control myotubes were only available from MHN individuals from family 1 (Control 01) and family 8 (Control 02). Myotubes from patients carrying the p.E2880K, p.R3772W and p.I4938T *RYR1* mutations (one myotube culture per patient and per mutation) and from the two controls were assessed for their sensitivity to KCl and 4-cmc and dose response curves were generated. Fig. 2 and Table 2 show that for both KCl and 4-cmc, cells carrying the p.E2880K (Fig. 2C and 2H) and p.R3772W (Fig. 2D and 2I) RyR1 mutations at the heterozygous state exhibited a significantly lower EC_{50} than cells from healthy controls, but neither PS3 nor PMa apply because of the unavailability of biological samples from at least 2 independent families. For cells carrying the p.I4938T RyR1 mutation, the EC_{50} of KCl was 18.1 ± 2.4 mM (Fig. 2E and Table 2) which is very similar and not significantly different to that of myotubes from control individuals, (18.5 ± 2.2 and 22.5 ± 12.2 mM, Fig. 2A and 2B and Table 2) and the EC_{50} for 4-cmc was higher (400.3 ± 52.6 µM, Fig. 2J and Table 2) compared to that of cells from control individuals (358.0 ± 46.5 and 310.0 ± 40.3 µM, Fig. 2F and 2G and Table 2), which supports its classification as "benign" (BS3_Sup). This discrepancy between agonist sensitivity and the presence of a putatively pathogenic RyR1 variant (p.I4938T), was not due to the absence of the mutation in the explanted myotubes, as its presence at the heterozygous state was confirmed by genomic DNA sequencing (Supplementary Fig. 1). The resting $[Ca^{2+}]_i$ in myotubes from controls and patients were not significantly different (Supplementary Fig. 2).

3.4. *Expression of recombinant p.G3806R, p.K4876R and p.I4938T RyR1 variants in HEK-293 cells and functional characterization of the mutations on [Ca^{2+}] homeostasis*

To confirm the presence of the full length RyR1 protomer western blot analysis was performed on microsomal fractions prepared from HEK-293 cells transfected with the WT and mutant *RYR1* cDNA,. The levels of expression of recombinant RyR1 protein were similar for the p.G3806R, p.K4876R and p.I4938T and WT constructs (Supplementary Fig. 3).

Since the transfection efficiency with a large cDNA construct such as that encompassing the *RYR1* cDNA (> 16 kbp) is relatively low, it is important to measure changes in $[Ca^{2+}]_i$ only in those cells expressing the recombinant RyR1 protein. For this reason, we subcloned the *RYR1* cDNA into the bi-cistronic pIRES2-DsRed2 vector, enabling the simultaneous expression of distinct proteins, namely DsRed (in the cytoplasm) and RyR1 (in the endoplasmic reticulum). Fig. 3 panels A and B, shows the results of a representative experiment. First HEK-293 cells were observed by brightfield microscopy (Fig. 3A upper left panel) then the same cells were observed by exciting the cells at 558 nm and recording the emission at 580 nm. As shown in the upper left panel, two cells are positive for the DsRed protein, indicating that they were transfected with the plasmid. Fig. 3A and B show respectively, the calcium-dependent fluorescence change and calcium transient elicited by the addition of 4-chloro-m-cresol in a DsRed transfected cell (arrowhead). Importantly, the RyR1 agonist did not cause an increase in fura-2 fluorescence in all cells, but rather only of those expressing the DsRed protein (time lapse ratiometric images are shown in the upper right panels of Fig. 3A). Using this method, we calculated the 4-cmc dose response curves for HEK-293 cells transfected with the p.G3806R (Fig. 3D), p.K4876R (Fig. 3E) and p.I4938T (Fig. 3F) RyR1 mutations and compared them to that obtained in cells transfected with the WT *RYR1* cDNA (Fig. 3C). The curves of all variant-transfected cells were shifted to the left relative to that of HEK-293 expressing WT RyR1 and the EC_{50} values were significantly lower in all variant-transfected cells than in HEK-293 expressing WT RyR1 (Table 3) supporting their pathogenicity (PSb).

We also measured the resting $[Ca^{2+}]$ in un-transfected HEK-293 cells and in cells transfected with the different constructs. Fig. 3G shows the box plots of the resting $[Ca^{2+}]$ and indicates that the $[Ca^{2+}]$ was significantly increased ($P < 0.001$ only in HEK-293 cells expressing the p.I4938T RyR1 variant, compared to cells expressing the WT RyR1.

3.5. *Variant classification*

After applying the results of this study, the classification of each variant based on the EMHG and VECP guidelines is summarized in Table 4.

4. Discussion

In this study, we performed functional analysis on five *RYR1* variants identified in IVCT-positive individuals. Our results show that myotubes obtained from patients carrying 2 out of 3 RyR1 mutations (p.E2880K and p.R3772W) were significantly more sensitive to KCl and 4-cmc stimulation compared to myotubes from control individuals. However, the agonist induced calcium release curves to KCl and 4-cmc in myotubes from the patient carrying the RyR1 p.I4938T variant were not more sensitive to agonist stimulation compared to myotubes from controls (BS3_Sup). This

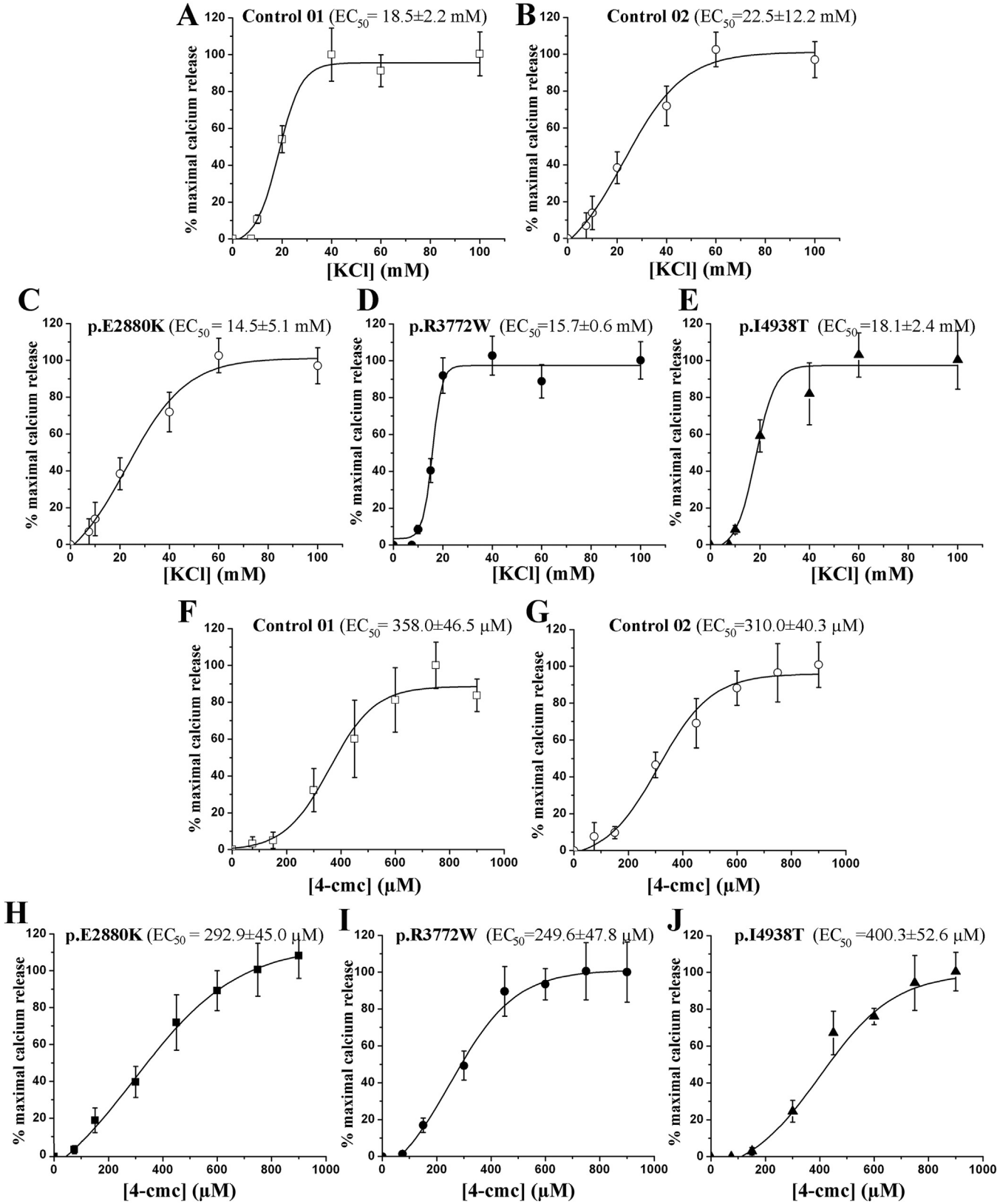

Fig. 2. KCl and 4-chloro-m-cresol dose-response curves of the ΔCa^{2+} in myotubes from controls and from patients with the indicated RyR1 mutations. The curves show the KCl (panels A–E) and 4-chloro-m-creol (panels F-J) dose-dependent changes in calcium, expressed as % maximal calcium release. Each point represents the mean (± S.E.M.) of the change in fluorescence in 6–12 myotubes. Data were normalized to the average peak calcium release obtained for the highest concentration of KCl or 4-chloro-*m*-cresol. Dose-response curves were generated using the Origin software. Myotubes obtained from 2 IVCT-negative individuals from family 1 and 8 were used as controls. The EC_{50} of variants p.E2880K and of p.R3772W are significantly lower than that of controls.

Table 4
Classification of variants based on EMHG and VCEP criteria.

Variant	EMHG Criteria	Classification	VCEP Criteria	Posterior possibility	Classification
c.8638 G >A p.E2880K	PMb, PPb, PPc	Likely pathogenic	PS4_Str, PP3_Mod, BS2_Mod	0.8993401	VUS
c.11314C>T p.R3772W	PMb, PPb, PPc	Likely pathogenic	PP3_Mod, PS4_Sup	0.5008319	VUS
c.11416G>A p.G3806R	PSb, PMb, PPa, PPb, PPc	Pathogenic	PS4_Str, PS3_Mod PP3_Mod	0.974631	Likely pathogenic
c.14627A>G p.K4876R	PSb, PMb, PPb, PPc	Pathogenic	PP3_Mod, PS3_Mod, PS4_Mod, PM1_Sup, PP1_Sup	0.974974	Likely pathogenic
c.14813T>C p.I4938T	PSb, PMb, PPb,	Pathogenic	PS3_Mod, PS3_Mod, PS4_Mod, PM1_Sup, BS3_Sup BS2_Mod	0.8991897	VUS

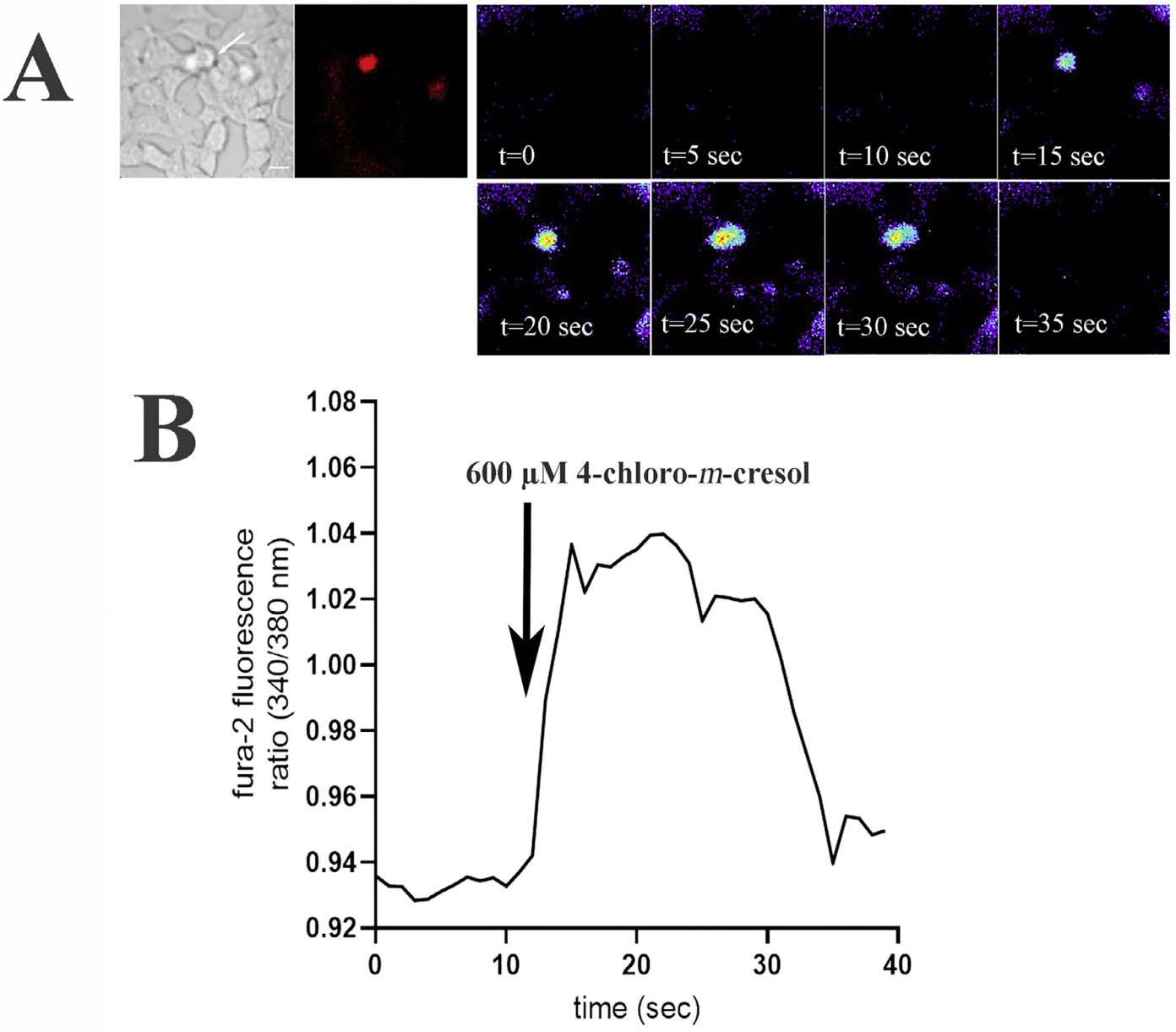

Fig. 3. Identification of DsRed *RYR1* transfected HEK-293 cells and 4-chloro-*m*-cresol dose-response curves of Ca^{2+} release in cells transfected with the human *RYR1* cDNA. **Part 1 (above)** A. The photomicrographs on the top portion of the figure show (starting from top left panel towards the right) brightfield image, the same image viewed at an excitation of 540 nm and emission of 575 nm. The remaining panels show the fura-2 fluorescent ratio changes following addition of 600 µM 4-chloro-m-cresol. The horizontal white bar shown in the upper left brightfield image = 10 µm **B.** Fura-2 ratio intensity (340/380 nm) over time following the application of 600 µM 4-chloro-m-cresol (in the cell indicated by the white arow in the top left panel)**. Part 2 (next page) C**. Dose-response curves of Ca^{2+} release in HEK-293 cells transfected with the human WT-*RYR1* cDNA in the bi-cistronic pIRES-DsRed vector. **D. E. and F.** Dose-response curves of Ca^{2+} release in HEK-293 cells transfected with the human *RYR1* cDNAs carrying the following variants: p.G3806R, p.K4876R and p.I4938T) in pIRES-DsRed vector. Data were normalized to the average peak calcium release obtained for the highest concentration of 4-chloro-*m*-cresol. Each point represents the mean (± S.E.M.) of the change in fluorescence of 4–40 measurements. Dose-response curves were generated using the Origin software. The curves of all variant-transfected cells were shifted to the left relative to that of HEK-293 expressing WT RyR1 and the EC_{50} values were significantly lower in all variant-transfected cells than in HEK-293 expressing WT RyR1. **G**. Resting [Ca^{2+}] (fura-2 fluorescence ratio) observed in HEK-293 cells. Each symbol represents the value of a single cell. P value of resting calcium between WT and I4938T < 0.0001.

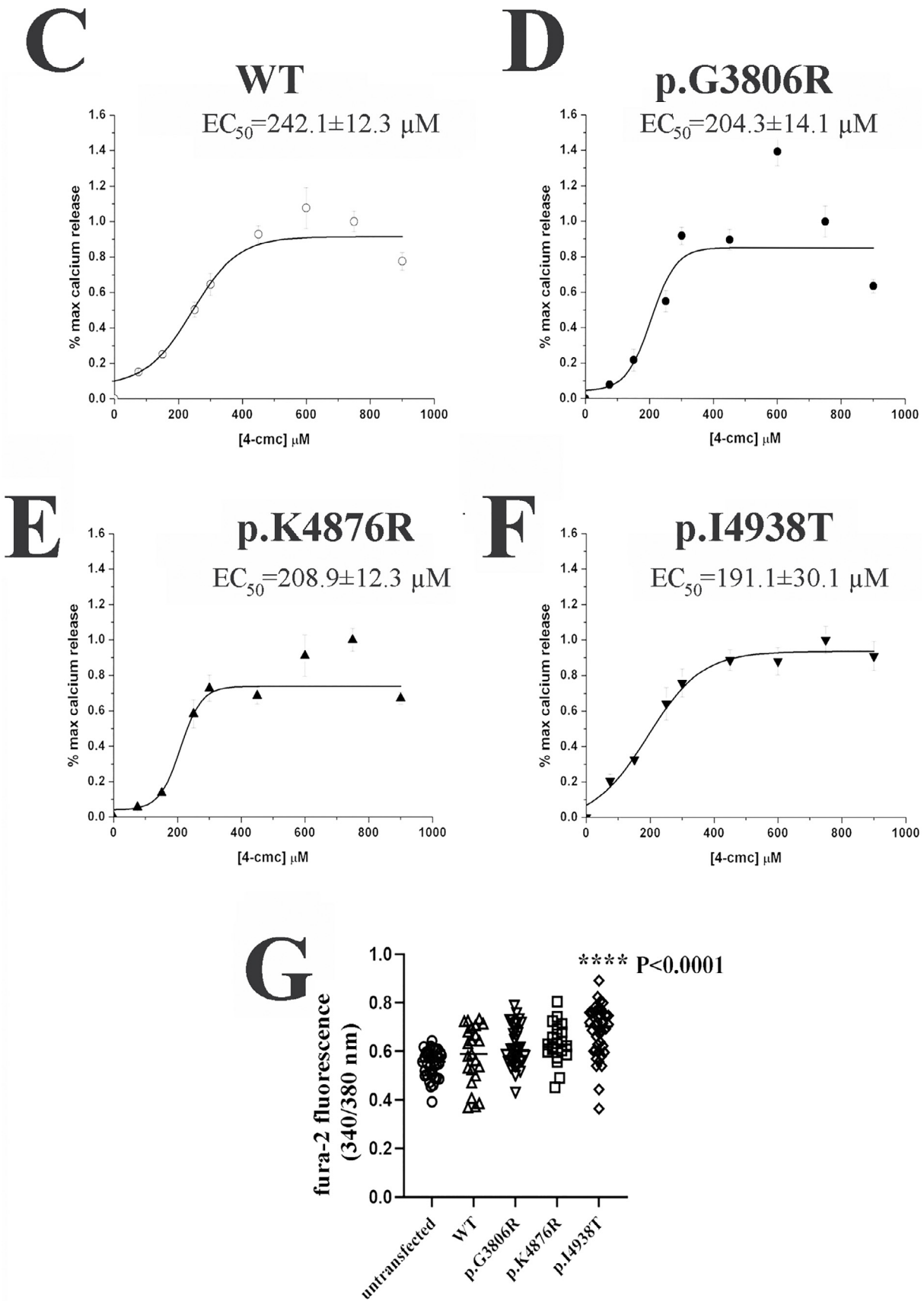

Fig. 3. Continued

discrepancy between agonist sensitivity and the presence of a putatively pathogenic RyR1 mutation was not due to the absence of the mutation in the myotubes, but may be caused by additional genetic factors affecting skeletal muscle calcium metabolism aside altered RyR1 function. Indeed, Yasuda et al., [32] showed that variants in *JSRP1*, the gene encoding JP-45, can counteract the hypersensitivity of EC coupling caused by *RYR1* mutations. Therefore, it is possible that the patient carrying the p.I4938T variant may carry mutations in other genes involved in excitation contraction coupling. Alternatively, the differential expression of mutant versus wild-type alleles in heterozygous patients, may be also possible. The latter explanation would also be compatible with the increased agonist sensitivity observed in transfected HEK-293 cells homozygous for the p.I4938T (PSb / PS3_Mod), not seen in heterozygous patient-derived myotubes (BS3_Sup).

Undoubtedly, myotubes explanted from patient biopsies may express unknown variants in other genes, therefore to study the isolated effect of the p.I4938T RyR1 mutation on calcium homeostasis, we inserted this mutation, as well as the two additional ones (p.G3806R and p. K4876R variants) found in the IVCT positive families from whom no cells were available, in the human *RYR1* cDNA and performed functional analysis on transfected HEK-293 cells expressing homozygous mutant channels. Our results confirm that the sensitivity to 4-cmc is significantly enhanced with each of the three variants, compared to cells expressing the WT RyR1 (PSb / PS3_Mod). Furthermore, the resting $[Ca^{2+}]_i$ was significantly elevated only in cells expressing the RyR1 p.I4938T mutation, indicating that the homozygous expression of this mutation most likely results in leaky channels. Elevation of the resting $[Ca^{2+}]_i$ has been previously reported in human myotubes from patients [19,33] EBV immortalized B-lymphocytes [34,35] carrying endogenous *RYR1* mutations, as well as in muscle cells expressing recombinant mutant RyR1 channels [36,37] and muscle cells from transgenic *Ryr1* mutant mice [38,39].

It is noteworthy that the p.I4938T RyR1 variant had a particularly large number of genotype-phenotype mismatches. Indeed: (i) the proband in the family developed an MH reaction but was not tested genetically nor tested by the IVCT; (ii) one individual carried the variant but was diagnosed as MHN by the IVCT; (iii) one individual did not carry this variant but was diagnosed as MHShc; (iv) two individuals who carried the variant were diagnosed as MHSh and one individual did not carry the variant and was also diagnosed as MHSh. Based on functional analysis using HEK-293 cells, the EC_{50} to 4-cmc of the p.I4938T variant was significantly lower compared to that of WT RyR1 (PSb / PS3_Mod), suggesting that the variant itself causes an abnormality in calcium homeostasis which is particularly evident when the mutation is expressed at the homozygous state. Nevertheless, one must also consider the possibility that in the family we investigated (family 8) the genotype-phenotype discrepancy may be due to the presence of mutations in other genes involved in calcium metabolism.

Once a variant is identified in an MHShc individual, all family members undergoing an IVCT are also tested for the presence or absence of the same variant. Therefore, other MH-causing variants may be present in the different family members. The results of several *in silico* predictive tools (Supplementary Table 1) [40] support the pathogenicity of all studied variants (PP3_Mod / PPb). Only p.E2280K was predicted to be benign by polyphen-2, but pathogenic using other prediction tool.

On a structural level, RyR1 is homotetramer with a molecular mass of more than 2.2MDa [41] and a large number of domains involved in the interaction with other proteins as well as the regulation of the calcium channel [26]. Fig. 4 models how the mutations identified in the MHS patients change the overall structure of the rabbit RyR1. All mutations reported in this paper were mapped in resolved regions of the protein structure and affect the Bsol, Csol and Pore domains (Fig. 4A). The first mutation, E2880K (rabbit: E2880), is located within the Bsol domain, in the cytosolic shell (CS, residues 1–3613) [33] of the receptor (Fig. 4A). The substitution of glutamate with lysine causes a change in the amino acid charge and results in two clashes, one with Y2908 and the other with E2876 (Fig. 4B). It seems that the structure accommodates the newly introduced amphipathic amino acid and changes the overall interactions as suggested by the possible clashes.

Mutation R3772W (rabbit: R3773) is located inside the channel and activation core (CAC, residues 3614–5037) of the receptor, precisely in the Csol domain (Fig. 4A), in proximity to the C-terminal domain (CTD) which contains among others, the calcium binding site. The calcium binding site is predominantly constituted by the interaction of five amino acids E3893, E3967, T5001, H3895 and Q3970 [26,42] and mutations therein or in surrounding residues may influence the activity of the Ca^{2+} channel [43]. The R3772 residue which is impacted by the mutation stands approximately 24 Å from the calcium binding site. While the amphipathic nature of the amino acid is maintained, the steric bulk of the tryptophan side chain could determine possible clashes with the nearby His3699 residue (Fig. 4C).

The mutation affecting the G3806R residue (rabbit: G3807) is also present inside the Csol domain, but in this case, it is closer to the calcium binding site than the R3772W mutation discussed above, at a distance of about 10 Å (Fig. 4A). The substitution of a small neutral amino acid like glycine, by a residue with a longer and more hydrophilic side chain such as arginine could theoretically influence the environment surrounding the calcium binding site as suggested by the possible clashes identified with L3763 (Fig. 4D).

Mutation K4876R (rabbit: K4875) resides in the bottom portion of the Pore domain of the channel (Fig. 4A). The substitution of the lysine side chain, with a stronger more positively charged and hydrophilic amino acid such as arginine, exposes a possible clash with the nearby F4885 and K4865 residues (Fig. 4E) and a possible consecutive change in the amino acid rearrangement.

Finally, mutation I4938T (rabbit: I4937) present in the central part of the Pore domain of the RyR1 (Fig. 4A), exposes the substitution of an uncharged and hydrophobic isoleucine residue with a hydrophilic threonine amino acid, which seems to be sterically accommodated and does not result in the presence of any additional clashes but rather a possible H-bond with residue Q4933 (Fig. 4F). The mutated amino acid is positioned between G4934 and G4941, which are two conserved residues composing the S6 pore-lining helix and are essential for RyR1 gating, since they convey the S6 flexibility, introducing a bend during the open or close states of the channel [44,45]. The increased hydrophilicity of the pore caused by the substitution of the hydrophobic isoleucine with the hydrophilic threonine, placed between the two essential glycine residues (i.e. Q4934 and Q4941) together with the destabilization made by the introduction of H-bonds with the Q4933 backbone, could determine a transition to the open conformation and/or higher conductance state [46].

One limitation of our study is that the functional analysis using myotubes was conducted on cells derived from one patient per family carrying the mutation. Although the results indicate a gain of function, the fact that they were derived from only one individual from one family prevents them from meeting the EMHG criteria for PMa and the modified ACMG/AMG criteria for *RYR1*-related MHS for PM3. Consequently, both mutations have to be classified as VUS according to the EMHG criteria and the modified ACMG/AMG criteria for *RYR1*-related MHS. Nevertheless, based on a paper categorizing *RYR1* variants according to ACMG/AMP [46], the criteria more frequently linked to Pathogenic or Likely

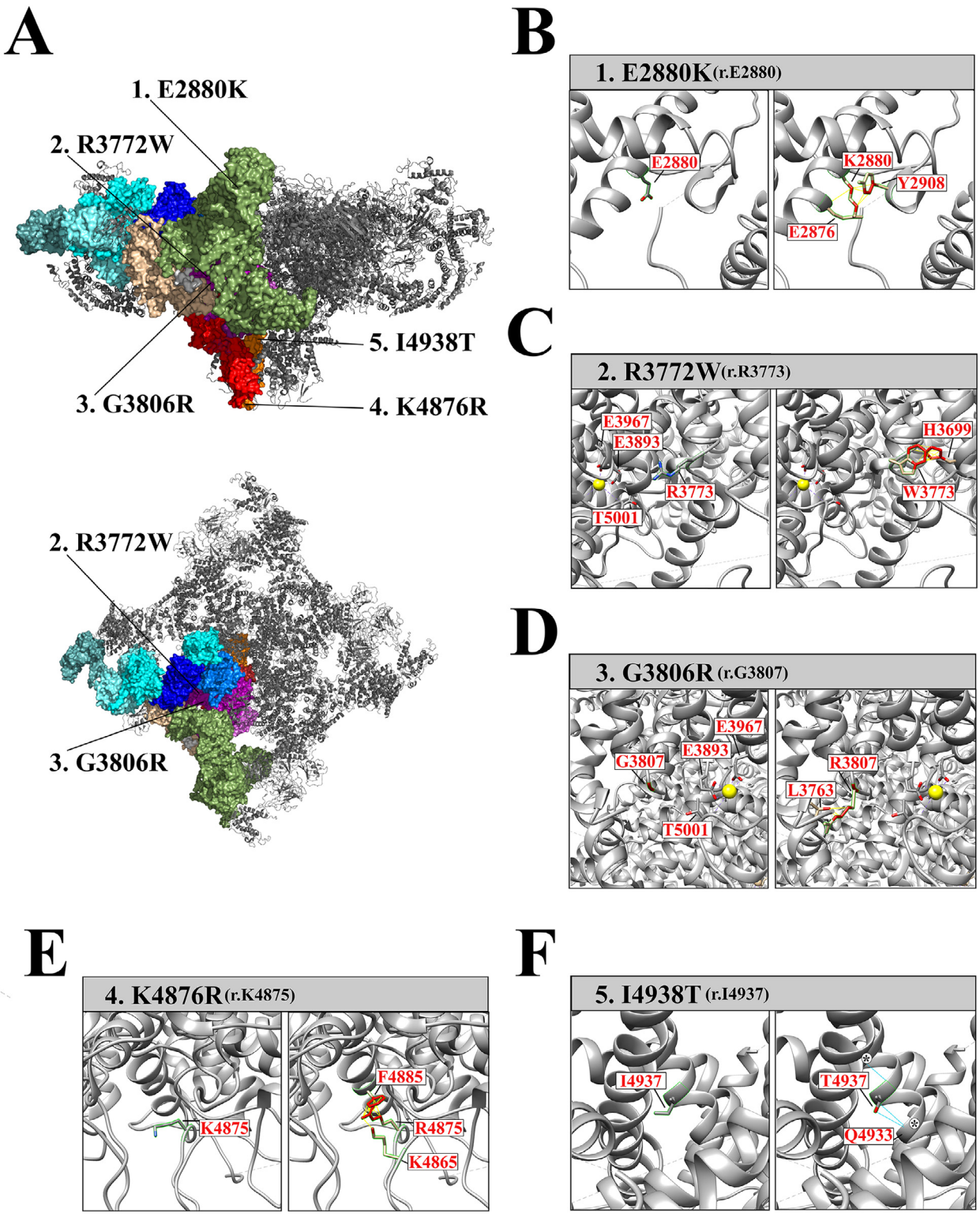

Fig. 4. 3D reconstruction of the RyR1 carrying the mutations described in the present investigation. **A**. Schematic representation of the various domains of the RyR1 and the respective position of the mutations. Specifically, E2880K (N°1) is in the Bsol, R3772W (N°2) and G3806R (N°3) are in the Csol, K4876R (N°4) and I4938T (N°5) are in the pore domain of the channel. PDB structure 5T15. **B**. Mutation of the native glutamate (left) into lysine (right). This substitution possibly results in clashes with Y2908 and E2876. **C**. Mutation R3772W is at an approximate distance of 24 Å from the calcium binding site and results in the possible clash with H3699. Amino acids within the calcium binding site such as E3967, E3893 and T5001 are also indicated. **D**. G3806R is 10 Å away from the calcium binding site and may cause clashes with L3763. Amino acids within the calcium binding site such as E3967, E3893 and T5001 are also indicated. **E**. K4876R shows two possible clashes, one with F4885 and the other with K4885 and the other with K4865. **F**. Substitution of isoleucine 4938 with threonine could result in the formation of an additional H bond with Q4933 backbone. Of note is the position of I4938 which is placed between G4934 and G4941 (indicated by asterisks), two residues that are important for channel gating. Panels B to F show the human and corresponding rabbit (r) mutations, respectively. The amino acids referred to in the text are shown in red and their numbers refer to the rabbit structure, PDB: 5TAL.

Pathogenic (in contrast to Benign, Likely Benign, or VUS) implicate the bioinformatics prediction of pathogenicity tool (REVEL scores of $\geq$ 0.85). Since, both variants identified as VUS in this study exhibited REVEL scores $\geq$ 0.85, they may be reevaluated as Pathogenic or Likely Pathogenic upon future investigations.

5. Conclusions

In conclusion, here we demonstrate that the 5 RyR1 variants investigated cause hypersensitivity to RyR1 agonist-mediated calcium release.

Abbreviations

IVCT	*In vitro* contracture test
EMHG	European Malignant Hyperthermia Group
MHN	Malignant hyperthermia negative
MHSEh	Malignant hyperthermia equivocal for Halothane
MHS	Malignant hyperthermia susceptible
RyR1	Ryanodine receptor 1

Author contribution

Y. N. performed experiments, prepared figures and helped writing the manuscript; H. M. performed experiments; S. B. performed the structural analysis and helped with the statistical analysis; A. G. performed the genetic analysis on patients and corrected the manuscript; O.B. and T. G. identified the patients, performed the IVCT, supervised the genetic analysis and corrected the manuscript; S.T. performed experiments, helped with the statistical analysis and helped writing the manuscript; F.Z. supervised Y.N., H.M and S. B., was involved in all aspects of the manuscript, including construct verification, statistical analysis and manuscript writing.

Ethical approval

This study was approved by the Ethics committee of the Basel University Hospital (EKNZ 2014–065) and patients donated their muscle biopsy to the biobank of the Swiss Muscle Foundation (https://muskel-stiftung.ch/index.php/welcome/information-en) for the purpose of MH associated research.

Declaration of Competing Interest

All authors declare that they have no conflict of interest.

Data availability

All data generated in this study is enclosed in the manuscript.

Acknowledgments

This work was supported by the Departments of Anesthesia of Hiroshima University hospital and Stiftung Anästhesiologie und Intensivmedizin, Basel, Switzerland. Molecular graphics and analyses performed with UCSF Chimera, developed by the Resource for Biocomputing, Visualization, and Informatics at the University of California, San Francisco, with support from NIH P41-GM103311.

Supplementary materials

Supplementary material associated with this article can be found, in the online version, at doi:10.1016/j.nmd.2023.10.019.

References

[1] Denborough M. Malignant hyperthermia. Lancet 1998;352:1131–6.
[2] MacLennan DH, Phillips MS. Malignant hyperthermia. Science 1992;256:789–94.
[3] Tomarken JL, Britt BA. Malignant hyperthermia. Ann Emerg Med 1987;16:1253–65.
[4] Ibarra Moreno C, Kraeva N, Zvaritch E, Jungbluth H, Voermans NC, Riazi S. Oral dantrolene for myopathic symptoms in malignant hyperthermia-susceptible patients: a 25-year retrospective cohort study of adverse effects and tolerability. Anesth Analg 2023;136:569–77.
[5] Krujit N, Van den Bersselaar L, Snoeck M, Kramers K, Riazi S, Bongers C, Treves S, Jungbluth H, Voermans NC. RYR1-related rhabdomyolysis: a spectrum of hypermetabolic states due to ryanodine receptor dysfunction. Curr Pharm Des 2022;28:2–14.
[6] Ohta T, Ito S, Ohga A. Inhibitory action of dantrolene on Ca-induced Ca2+ release from sarcoplasmic reticulum in guinea pig skeletal muscle. Eur J Pharmacol 1990;178:11–19.
[7] Parness J, Palnitkar SS. Identification of dantrolene binding sites in porcine skeletal muscle sarcoplasmic reticulum. J Biol Chem 1995;270:18465–72.
[8] Noda Y, Mukaida K, Miyoshi H, Nakamura R, Yasuda T, Saeki N, Nishino I, Tsutsumi YM. The effects of dantrolene in the presence or absence of ryanodine receptor type 1 variants in individuals predisposed to malignant hyperthermia. Anaesth Intensive Care 2022;50:312–19.
[9] Islander G, Ording H, Bendixen D, Ranklev Twetman E. Reproducibility of *in vitro* contracture test results in patients tested for malignant hyperthermia susceptibility. Acta Anaesthesiol Scand 2002;46:1144–9.
[10] Hopkins PM, Rüffert H, Snoeck MM, Girard T, Glahn KPE, Ellis FR, Müller CR, Urwyler A. European malignant hyperthermia group guidelines for investigation of malignant hyperthermia susceptibility. Br J Anaesth 2015;115:531–9.
[11] Robinson RL, Anetseder MJ, Brancadoro V, van Broekhoven C, Carsana A, Censier K, et al. Recent advances in the diagnosis of malignant hyperthermia susceptibility: how confident can we be of genetic testing? Eur J Hum Genet 2003;11:342–8.
[12] Beam T, Loudermilk EF, Kisor DF. Pharmacogenetics and pathophysiology of CACNA1S mutations in malignant hyperthermia. Physiol Genomics 2017;49:81–7.
[13] Miller DM, Daly C, Aboelsaod EM, Gardner L, Hobson SJ, Riasat K, Shepherd S, et al. Genetic epidemiology of malignant hyperthermia in the UK. Br J Anaesth 2018;121:944–52.
[14] Rosenberg H, Pollock N, Schiemann A, Bulger T, Stowel K. Malignant hyperthermia: a review. Orphanet J Rare Dis 2015. doi:10.1186/s13023-015-0310-1.
[15] Johnston JJ, Dirksen RT, Girard T, Gonsalves SG, Hopkins PM, Riazi S, et al. Variant curation expert panel recommendations for RYR1 pathogenicity classifications in malignant Hyperthermia susceptibility. Genet Med 2021;23:1288–95.
[16] Garcia FAO, de Andrade ES, Palmero EI. Insights on variant analysis in silico tools for pathogenicity prediction. Front Genet 2022;13:1010327.
[17] Tavtigian SV, Greenblatt MS, Harrison SM, Nussbaum RL, Prabhu SA, Boucher KM, Biesecker LG. Modeling the ACMG/AMP variant classification guidelines as Bayesian classification frameworks. Genet Med 2018;20(9):1054–60 Sep.
[18] Censier K, Urwyler A, Zorzato F, Treves S. Intracellular calcium homeostasis in human primary muscle cells from malignant hyperthermia-susceptible and normal individuals. Effect Of overexpression of recombinant wild-type and Arg163Cys mutated ryanodine receptors. J Clin Invest 1998;101:1233–42.
[19] Ducreux S, Zorzato F, Müller C, Sewry C, Muntoni F, Quinlivan R, et al. Effect of ryanodine receptor mutations on interleukin-6 release and intracellular calcium homeostasis in human myotubes from malignant hyperthermia-susceptible individuals and patients affected by central core disease. J Biol Chem 2004;279:43838–46.
[20] Treves S, Girard T, Zorzato F. Functional characterization of endogenously expressed human RYR1 variants. J Vis Exp 2021. doi:10.3791/62196.
[21] Treves S, Pouliquin P, Moccagatta L, Zorzato F. Functional properties of EGFP-tagged skeletal muscle calcium-release channel (ryanodine receptor) expressed in COS-7 cells: sensitivity to caffeine and 4-chloro-m-cresol. Cell Calcium 2001;31:1–12.
[22] Treves S, Larini F, Menegazzi P, Steinberg TH, Koval M, Vilsen B, et al. Alteration of intracellular Ca^{2+} transients in COS-7 cells transfected with the cDNA encoding skeletal-muscle ryanodine receptor carrying a mutation associated with malignant hyperthermia. Biochem J 1994;301:661–5.
[23] Rokach O, Sekulic-Jablanovic M, Voermans N, Wilmshurst J, Pillay K, Heytens L, et al. Epigenetic changes as a common trigger of muscle weakness in congenitl myopathies. Hum Mol Genet 2015;24:4636–47.
[24] Pettersen EF, Goddard TD, Huang CC, Couch GS, Greenblatt DM, Meng EC, Ferrin T. EUCSF Chimera–a visualization system for exploratory research and analysis. J Comput Chem 2004;25:1605–12.
[25] Shapovalov MV, Dunbrack RL Jr. A smoothed backbone-dependent rotamer library for proteins derived from adaptive kernel density estimates and regressions. Structure 2011;19:844–58.
[26] des Georges A, Clarke OB, Zalk R, Yuan Q, Condon KJ, Grassucci RA, et al. Structural basis for gating and activation of RyR1. Cell 2016;167:145–57.
[27] ww PDB consortiumProtein Data Bank: the single global archive for 3D macromolecular structure data. Nucleic Acids Res 2019;47(D1):D520–8.

[28] Levano S, Vukcevic M, Singer M, Matter A, Treves S, Urwyler A, Girard T. Increasing the number of diagnostic mutations in malignant hyperthermia. Hum Mutat 2009;30:590–8.
[29] Monnier N, Kozak-Ribberns G, Krivosic-Horber R, Nivoche Y, Qi D, Kraev N, et al. Correlations between genotype and pharmacological, functional, and clinical phenotypes in malignant hyperthermia susceptibility. Hum Mutat 2005;26:413–25.
[30] Shaaban S, Ramos-Platt L, Gilles FH, Chan WM, Andrew C, De Girolami U, et al. RYR1 mutations as a cause of ophthalmoplegia, facial weakness, and malignant hyperthermia. JAMA Ophthalmol 2013;13:1532–40.
[31] Ioannidis NM, Rothstein JH, Pejaver V, Middha S, McDonnell SK, Baheti S, et al. REVEL: an ensemble method for predicting the pathogenicity of rare missense variants. Am J Hum Genet 2016;99:877–85.
[32] Yasuda T, Delbono O, Wang ZM, Messi ML, Girard T, Urwyler A, Treves S, Zorzato F. JP-45/JSRP1 variants affect skeletal muscle excitation-contraction coupling by decreasing the sensitivity of the dihydropyridine receptor. Hum Mutat 2013;34:184–90.
[33] Zhou H, Yamaguchi N, Xu L, Wang Y, Sewry C, Jungbluth H, et al. Characterization of recessive RYR1 mutations in core myopathies. Hum Mol Genet 2006;15:2791–803.
[34] Girard T, Cavagna D, Padovan E, Spagnoli G, Urwyler A, Zorzato F, Treves S. B-lymphocytes from malignant hyperthermia-susceptible patients have an increased sensitivity to skeletal muscle ryanodine receptor activators. J Biol Chem 2001;276:48077–82.
[35] Ducreux S, Zorzato F, Ferreiro A, Jungbluth H, Muntoni F, Monnier N, et al. Functional properties of ryanodine receptors carrying three amino acid substitutions identified in patients affected by multi-minicore disease and central core disease, expressed in immortalized lymphocytes. Biochem J 2006;395:259–66.
[36] Yang T, Allen PD, Pessah IN, Lopez JR. Enhanced excitation-coupled calcium entry in myotubes is associated with expression of RyR1 malignant hyperthermia mutations. J Biol Chem 2007;282:37471–8.
[37] Avila G, Dirksen RT. Functional effects of central core disease mutations in the cytoplasmic region of the skeletal muscle ryanodine receptor. J Gen Physiol 2001;118:277–90.
[38] Feng W, Barrientos GC, Cherednichenko G, Yang T, Padilla IT, Truong K, et al. Functional and biochemical properties of ryanodine receptor type 1 channels from heterozygous R163C malignant hyperthermia-susceptible mice. Mol Pharmacol 2011;79:420–31.
[39] Yuen B, Boncompagni S, Feng W, Yang T, Lopez JR, Matthaei KI, et al. Mice expressing T4826I-RYR1 are viable but exhibit sex- and genotype-dependent susceptibility to malignant hyperthermia and muscle damage. FASEB J 2012;26:1311–22.
[40] Johnston JJ, Dirksen RT, Girard T, Hopkins PM, Kraeva N, Ognoon M, Radenbaugh KB, Riazi S, Robinson RL, Saddic Iii LA, Sambuughin N, Saxena R, Shepherd S, Stowell K, Weber J, Yoo S, Rosenberg H, Biesecker LG. Updated variant curation expert panel criteria and pathogenicity classifications for 251 variants for RYR1-related malignant hyperthermia susceptibility. Hum Mol Genet 2022;31:4087–93.
[41] Chen W, Kudryashev M. Structure of RyR1 in native membranes. EMBO Rep 2020;21(5):e49891. doi:10.15252/embr.201949891.
[42] Chang X, Wei R, Wei C, Liu J, Qin L, Yan H, et al. Correlation of phenotype-genotype and protein structure in RYR1-related myopathy. Front Neurol 2022;13:870285. doi:10.3389/fneur.2022.870285.
[43] Yuan Q, Dridi H, Clarke OB, Reiken S, Melville Z, Wronska A, et al. RyR1-related myopathy mutations in ATP and calcium binding sites impair channel regulation. Acta Neuropathol Commun 2021;9(1):186. doi:10.1186/s40478-021-01287-3.
[44] Mei Y, Xu L, Mowrey DD, Mendez-Giraldez R, Wang Y, Pasek DA, et al. Channel gating dependence on pore lining helix glycine residues in skeletal muscle ryanodine receptor. J Biol Chem 2015;290:17535–45.
[45] Xu L, Mowrey DD, Chirasani VR, Wang Y, Pasek DA, Dokholyan NV, Meissner G. G4941K substitution in the pore-lining S6 helix of the skeletal muscle ryanodine receptor increases RyR1 sensitivity to cytosolic and lumina, Ca^{2+}. J Biol Chem 2018;293:2015–28.
[46] Yonkunas M, Kurinikova M. The hydrophobic effect contributes to the closed state of a simplified ion channel through a conserved hydrophobic patch at the pore-helix crossing. Front Pharmacol 2015;6:284. doi:10.3389/fphar.2015.00284.